

Article

# Optimization of Bio-Hydrogenated Kerosene from Refined Palm Oil by Catalytic Hydrocracking

Praepilas Dujjanutat <sup>1</sup>, Arthit Neramittagapong <sup>2,3</sup> and Pakawadee Kaewkannetra <sup>3,\*</sup>

<sup>1</sup> Graduate School of Khon Kaen University, Khon Kaen 40002, Thailand

<sup>2</sup> Department of Chemical Engineering, Faculty of Engineering, Khon Kaen University, Khon Kaen 40002, Thailand

<sup>3</sup> Center of Alternative Energy Research and Development (AERD), Faculty of Engineering, Khon Kaen University, Khon Kaen 40002, Thailand

\* Correspondence: pakawadee.kku@gmail.com

Received: 18 June 2019; Accepted: 17 August 2019; Published: 20 August 2019



**Abstract:** In this work, hydro-processing was used as an alternative route for producing bio-hydrogenated kerosene (BHK) from refined bleached deodorized palm oil (RPO) in the presence of a 0.5 wt% Pd/Al<sub>2</sub>O<sub>3</sub> catalyst. The Box-Behnken Design was used to determine the effects of reaction temperature, H<sub>2</sub> pressure, and reaction time in terms of liquid hourly space velocity (LHSV) on BHK production. The kerosene selectivity was used as the response for statistical interpretation. The results show that both temperature and LHSV produced significant effects, whereas H<sub>2</sub> pressure did not. The optimal conditions were found to be 483 °C, 5.0 MPa, and 1.4 h<sup>-1</sup> LHSV; these conditions provided approximately 57.30% kerosene selectivity and a 47.46% yield. The BHK product had a good heating value and flash point. However, the mass percentage of carbon and hydrogen was 99.1%, which is just below the minimum standard (99.5%), according to the carbon loss by the reaction pathway to form as CO and CO<sub>2</sub>. Water can be produced from the reaction induced by oxygen removal, which results in a high freezing point.

**Keywords:** hydrocracking reaction; bio-hydrogenated kerosene (BHK); refined bleached deodorized palm oil (RPO); Box-Behnken Design (BBD); kerosene

## 1. Introduction

Worldwide population growth has led to increased numbers of automobiles and air vehicles, which has rapidly increased global energy consumption. This demand for petroleum fuels has rapidly depleted the world's reserves and has raised energy prices and increased environmental concerns. Due to the unsustainability of petroleum-based fuel, biofuel derived from renewable resources plays an important role in meeting long-term energy demands if managed efficiently and generates almost no net greenhouse gases [1].

Bio-hydrogenated kerosene (BHK), a flammable renewable liquid hydrocarbon produced via hydrocracking, may replace kerosene. BHK has better properties than fossil fuels and can be produced from bio-based raw materials such as vegetable oils and animal fats that contain triglyceride (TG) and are free of sulfur-containing compounds. Therefore, BHK can be classified as an environmentally friendly product [2,3]. BHK also generates less pollution during combustion than kerosene [4] and has similar physical properties to kerosene. For example, the boiling point of BHK is normally 172–263 °C, whereas that of kerosene is 170–300 °C [5]. However, the product selectivity of hydrocracking depends on the reaction conditions and catalyst selection [6]. Catalyst selection can indicate the side reactions and provide higher selectivity of the desired product. Normally, noble metal catalysts (Pt and Pd) are suitable for use in hydrocracking reactions because they are sensitive to sulfur, which can lead

to catalyst deactivation. Therefore, feedstock used together with a catalyst should be free of sulfur. Noble metals have been widely reported as active metals in hydro/dehydrogenation and isomerization reactions, requiring much lower amounts of metal compared to Ni [7,8].

Given the conventional fuel situation and catalyst sensitivity, TGs are a suitable feedstock for biofuel production via hydro-processing. TGs contain various hydrocarbons related to several types of biofuel. The chain length of fatty acids in natural TG is variable; however, the chain usually contains two to 28 carbon atoms. This led to the idea that the chain of fatty acids can be changed to create a new structure containing fewer carbon atoms than the original compounds and that their characteristics as a fuel can be determined. Typically, kerosene contains hydrocarbons  $C_9$ – $C_{14}$  in its structure, which is related to the fatty acid's structure, as described above [9]. Compared with other vegetable oils in international markets, palm oil shows the highest yield production due to its ability to grow under tropical climate conditions. It is mostly used as a raw material for biodiesel production in Southeast Asia [10].

Typically, the main compositions of palm oil are a 16-carbon atom saturated palmitic acid and an 18-carbon atom monounsaturated oleic acid, both of which are found in equal amounts of about 42% [11]. The many impurities in crude palm oil (CPO), produced during the milling process, must be removed by a refining process, as simply explained in Figure 1. In brief, oil palm is crushed in an oil pressing machine to extract the oil. Water and contaminants are filtered, the oil is fed to the dehumidifying machine, and the CPO is obtained. Then, it is further processed for degumming, bleaching, and deodorizing. Subsequently, palm fatty acid distillate (PFAD) and deodorized palm oil (RPO) were obtained. Only the RPO is further refined to produce the highest purity refined bleached deodorized palm olein (RPOL; food grade) using a fractionation process to separate solid palm stearin and produce refined bleached deodorized palm stearin (RPS). However, RPS has a solid fraction with a high melting point that is not suitable for use as a feedstock for producing biofuel under the up-flow reactor system due to its soft solid state at room conditions. This augments the required pumping power and creates clogging in the tubular line of the reactor. Many researchers have studied both CPO and RPOL. Even though RPOL has been reported as an appropriate feedstock, it is more expensive than the others and is best for use in home cooking. Therefore, searching for other available sources to formulate biofuels is necessary; one of the more unexplored sources of feedstock is RPO. This bio-based feedstock has characteristics similar to RPOL but it is less pure and is cheaper. RPO has already been used in instant noodles, margarine, and shortening products.

The Box-Behnken Design (BBD) can be used for the design of experiments (DOEs) based on response surface methodology (RSM) to interpret the operating parameters for process optimization. BBD can be applied to determine levels of design parameters that would result in the optimum value of the response. Benefits of the BBD are that a large amount of complex information can be obtained, reducing experimental time as well as the required materials and costs [12].

Therefore, in this work, RPO obtained from the palm oil refinery process was used as a raw material for producing BHK via hydrocracking. BBD was used as a tool to determine the optimal conditions for BHK production. The product obtained was evaluated in terms of its properties compared to the properties of commercial kerosene following the USA military specification based on the American Society for Testing and Materials (ASTM) international standard.

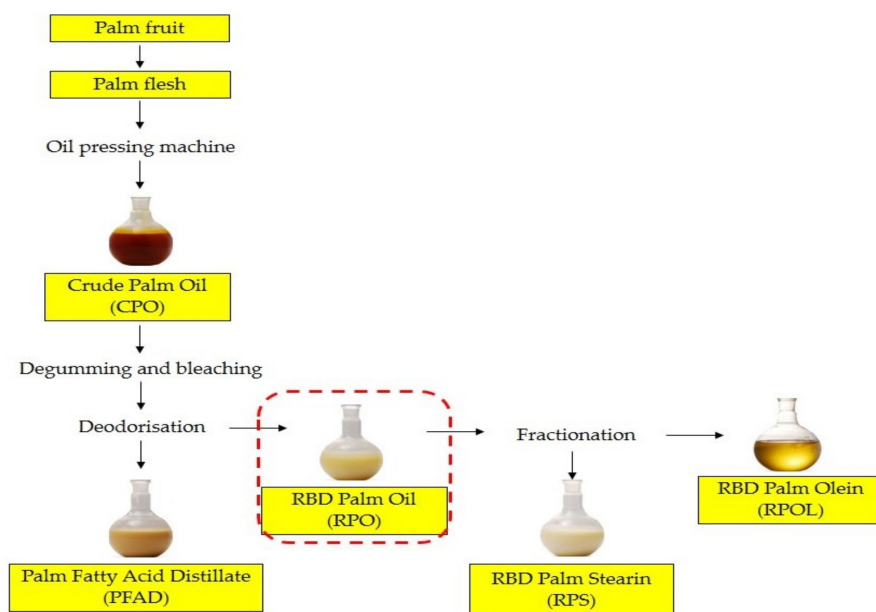


**Figure 1.** The refinery palm oil process. Refined palm oil (RPO), seen within the red dashed box, was used as feedstock. RBD is an abbreviation of refined, bleached, and deodorized.

## 2. Materials and Methods

### 2.1. Materials

The RPO produced from the refinery line process of the palm oil industry, described in Figure 1, was kindly provided by Chumporn Palm Oil Industry (Chumporn, Thailand). Hydrogen gas (95% purity) was used as the injection gas during the reaction and 99.999% pure nitrogen gas was used for checking for gas leaks in the system and cooling the reaction. A commercial grade 0.5% Pd/Al<sub>2</sub>O<sub>3</sub> catalyst was purchased from Heze Development Zone Dayuan Chemical Co., Ltd., Zhejiang, China, and was used throughout the hydrocracking reaction.

### 2.2. Catalyst Characterization

Specific surface area and related data were estimated based on the Brunauer–Emmett–Teller (BET) method. The catalyst was analyzed using the nitrogen adsorption-desorption isotherm at  $-196.1\text{ }^{\circ}\text{C}$  in an ASAP 2020 instrument (Micromeritics, Norcross, GA, USA). Prior to the analysis, the catalyst was outgassed at  $120\text{ }^{\circ}\text{C}$  for 3 h. The crystallite structure of the Pd/Al<sub>2</sub>O<sub>3</sub> catalyst was measured by an X-ray diffractometer (XRD) in a PANalytical X'pert Pro instrument (Malvern Panalytical Ltd., Royston, United Kingdom) using Cu-K $\alpha$  radiation at  $\lambda = 1.542\text{ \AA}$ , and operating at 40 kV, 40 mA, and an incremental step size of  $0.0167^{\circ}$  with a step time of 100 s in the range of  $10^{\circ}$  to  $90^{\circ}$ . SEM images of fresh and spent catalysts were captured with an FEI Quanta 200 (Thermo Fisher Scientific, Waltham, MA, USA).

### 2.3. Reaction and DOE

A high-pressure packed bed reactor (HPPBR) was used for operating the hydrocracking reaction. The details of the reactor have been described previously [13]. In brief, it consisted of three main systems: a feed system, a reactor reaction system, and a product separation system, as illustrated in Figure 2.

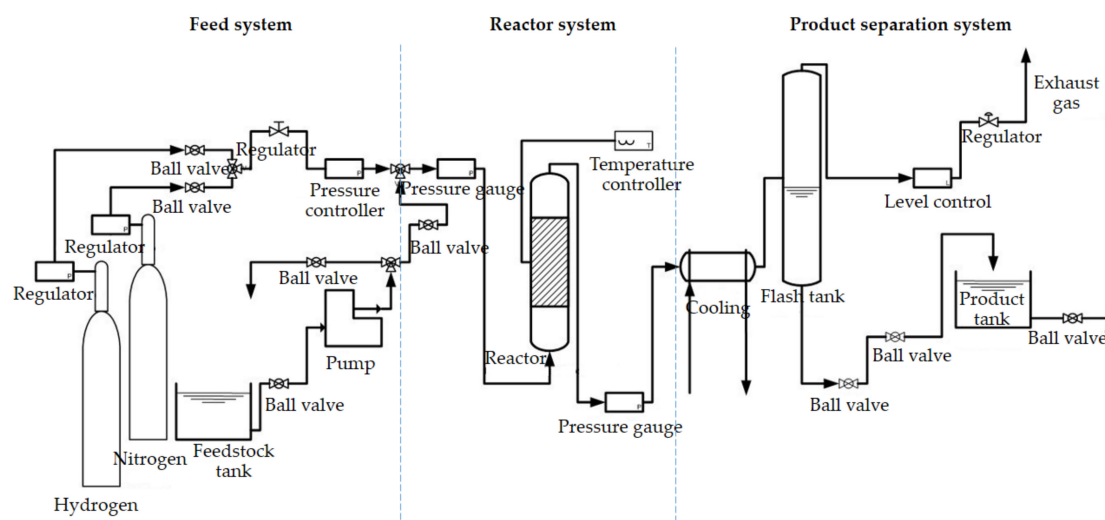


**Figure 2.** Diagram of high pressure packed bed reactor (HPPBR).

The feedstock tank, feed pump, and gas cylinders, including regulators, were the feed system accessories. RPO was stored in the feedstock tank and fed by the feed pump and mixed with H<sub>2</sub> before entering the second system. The reactor was composed of a stainless steel tube with a 100 mL working volume and the catalyst was packed inside the tube. The hydrocracking occurred in the system. The operating temperature was controlled by two thermocouples installed at the top and bottom of the reactor. Temperature and pressure were strictly controlled to produce severe conditions, while the feedstock flow rate was controlled by the feed pump and the flow meter controlled the gas. RPO and H<sub>2</sub> were mixed and fed into the reactor at the bottom of the reactor. Finally, the hydroprocessed biofuel product was exported from the top of the reactor (up-flow current), and continually flowed to condense at the heat exchanger to separate the liquid and gas in the third part of the product separation system. The liquid product could be harvested from a product tank and was further separated by distillation and gases were released to the atmosphere.

Three factors, namely, temperature, pressure, and liquid hourly space velocity (LHSV), were investigated to determine their effects using the BBD, the ranges of which are presented in Table 1. This method was evaluated using Minitab 16 statistical software (Minitab, Inc., State College, PA, USA). We conducted 15 experimental runs following the DOE. After the reaction, the hydroprocessed product was collected and filtered using Whatman filter paper No. 1. Then, the BHK was separated using the distillation method (ASTM D86 standard) [14]. The kerosene selectivity was considered the response to be optimized and was also evaluated using the Minitab program (Minitab Inc., State College, PA, USA).

**Table 1.** The ranges of values of the investigated factors used for the experimental design.

Variable	Low (−)	Medium (0)	High (+)
Temperature ( $X_1$ ; °C)	450	500	550
Pressure ( $X_2$ ; MPa)	4	5	6
LHSV ( $X_3$ ; h <sup>−1</sup> )	0.5	1.0	1.5

Legend LHSV, liquid hourly space velocity.

#### 2.4. Bio-Hydrogenated Kerosene Properties

The BHK properties were analyzed following the ASTM standard and compared with the specification of kerosene-type aviation fuel MIL-DTL-83133H. This specification was issued by the US military due to the military-specific nature of the products and the details provided are specific to TG-derived kerosene produced by hydroprocessing. However, the specification is also based on the global ASTM standard for approval of alternative aviation fuel. For detailed analysis, carbon and

hydrogen were analyzed following the ASTM D5291 protocol, whereas the nitrogen composition was determined following ASTM D4629 and oxygen was also calculated from the differences between carbon and nitrogen. The freezing point value was evaluated following ASTM D2386 and the carbon distribution in the BHK product was analyzed via a gas chromatography-flame ionization detector (GC-FID) following the Universal Oil Products standard (UOP 915).

### 3. Results and Discussion

#### 3.1. Catalyst Characterization

The physical properties of the catalyst were characterized using the BET method. The surface area was  $75.3 \text{ m}^2/\text{g}$ , whereas the pore volume of the catalyst was about  $0.16 \text{ cm}^3/\text{g}$ . The average pore diameter was  $7.5 \text{ nm}$ , meaning the catalyst may be classified as a mesoporous material. This was confirmed by the nitrogen sorption isotherm (Figure 3). We observed a type IV isotherm curve at a relative pressure  $P/P^0$  of  $0.04\text{--}0.99$ , which led to the identification of a mesoporous catalyst with pore diameters between  $2$  and  $50 \text{ nm}$  according to the IUPAC classification [15]. The pore diameter of the catalyst can readily allow the diffusion of the bulky TG molecule of palm oil. Tiwari et al. have estimated TG dimensions from the dimensions of methyl oleate and glycerol as being between  $2.5 \text{ nm}$  and  $0.6 \text{ nm}$  in length [16]. According to them, methyl oleate and glycerol have a correlation dimension with the TG molecule. TG could enter the pore of a catalyst that was larger than both TG and the fatty acid chain, so the reaction was able to occur in the active site of the catalyst. We concluded that the mesoporosity of the catalyst is important for producing BHK by hydrocracking when using TG as feedstock because it offers moderate acidity, and the desired surface area and pore diameter are suitable for producing middle distillate hydrocarbons. The results obtained are in agreement with those of Looi et al. who have explained that the pore structure of the catalyst plays an important role in the reaction activity and selectivity of distillate products [7].

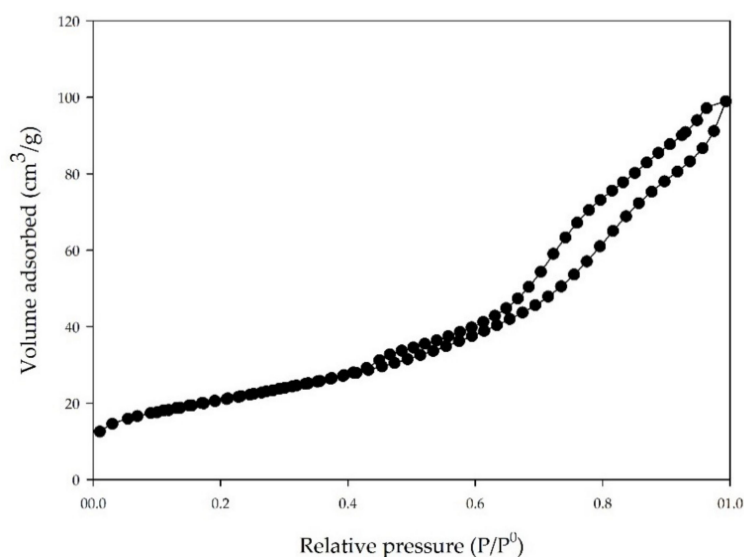


**Figure 3.** Nitrogen sorption isotherm of mesoporous Pd/Al<sub>2</sub>O<sub>3</sub>.

However, micropore volume also affects the reaction by affecting the access of the TG bulk. A catalyst with high pore volume, high surface area, and large pore size distribution would be better for reacting with TG and producing high reaction activity. Deactivation of the catalyst occurs from the occurrences of coke and the waxy intermediates during the reaction, and these could be resulted to a pore blockage situation [17]. The type of reactor also affects this problem. Ancheyta et al. have reported that the drawback with using a fixed-bed reactor is metal accumulation and coke blockage in the catalytic pores that can obstruct the access of reactants to the internal surface [6]. However,

the problem was able to be solved in this work by in situ burning of the catalyst (regeneration) with zero air gas at 420 °C for three hours. Then, the temperature was increased to 500 °C for two hours. The morphology of the catalyst was studied both before and after hydrocracking of RPO (Figure 4). The dispersed Pd metal particles were observed in both fresh and spent catalysts, which were located mainly on the surface of the supporting material. We concluded that the severe hydrocracking reaction conditions did not influence the metal particles and the sintering of Pd particles did not occur.

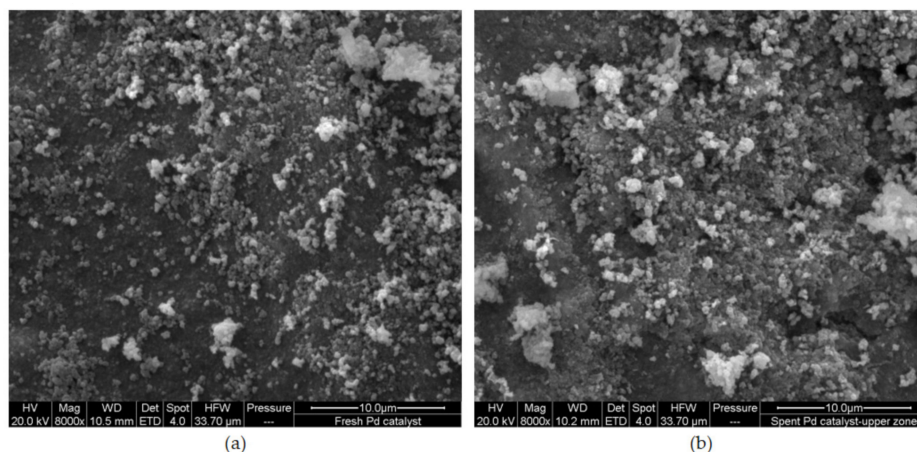


**Figure 4.** SEM images of (a) fresh and (b) spent Pd/Al<sub>2</sub>O<sub>3</sub> catalysts (×8000 magnification).

The XRD pattern of the Pd/Al<sub>2</sub>O<sub>3</sub> catalyst was examined and is presented in Figure 5. The catalyst showed a crystalline structure in narrow and intense diffraction peaks of Al<sub>2</sub>O<sub>3</sub>, TiO<sub>2</sub>, and PdO. The discovery of TiO<sub>2</sub> in the XRD pattern was unexpected. Perhaps a titanium compound was added into the catalyst during the production. The discovery of titanium explains the low specific surface area of the catalyst [18]. However, the titanium may have improved the catalyst. Some previous works have tried to use titanium for hydro-processing and TiO<sub>2</sub>-supported metal catalysts have been reported to produce higher hydrodesulfurization activity compared to those supported by Al<sub>2</sub>O<sub>3</sub> [19–21]. Similar information has also been reported by Castillo-Villalón et al. Enhanced Mo/TiO<sub>2</sub> catalyst activity has been seen to produce a slight increase in direct desulfurization while significantly enhancing hydrogenation [22]. Synergy usually occurs between the support and the active metal components of the hydrocracking catalyst with the use of titanium as opposed to aluminum. In addition, TiO<sub>2</sub> has been found to be an unsuitable support for use at high temperatures due to its low specific surface area, low mechanical strength, and low thermal stability of the active anatase structure [18,23]. Therefore, the support should be composed of a mix oxides of TiO<sub>2</sub> and Al<sub>2</sub>O<sub>3</sub> to take advantage of the beneficial features of both oxides and to produce a higher catalytic activity [18].

### 3.2. Reaction and Optimization

The HPPBR was operated at different reaction temperatures, pressures, and LHSV following the BBD, as shown in Table 2. The crude biofuel product obtained from every run was collected from the reactor from a terminal port of the product storage tank and subsequently refined by distillation following the ASTM D86 standard for separating BHK. The selectivity of kerosene was calculated by Equation (1) and is shown in Table 2. We determined the optimal conditions for the BHK production using response surface methodology (RSM) within the BBD tool.

$$KS = \frac{B}{D} \times 100 \quad (1)$$

where *KS* is kerosene selectivity, *B* is the volume of the BHK fraction with a boiling point between 150 and 280 °C, and *D* is the volume of all distillate products under 360 °C. Notably, the distillate over 360

°C was classified as a heavy oil and was not included in the distillate product. The boiling point of the light oil and middle distillate started from 50 °C and ended at 360 °C, with BHK included in this range. Minitab (Minitab, Inc., State College, PA, USA) was used to interpret the direct and interactive effects of process parameters (temperature, pressure, and LHSV) on BHK production. The results were used to identify the significant and non-significant terms of all parameters and the second-order mathematical model is illustrated in Equation (2). The non-significant terms have been removed.

$$Y = 52.86 - 11.66X_1 + 6.49X_3 - 12.11X_1^2 \quad (2)$$

where  $Y$  is the kerosene selectivity (%) and  $X_1$ ,  $X_2$ , and  $X_3$  are the coded values of temperature, pressure, and LHSV, respectively.

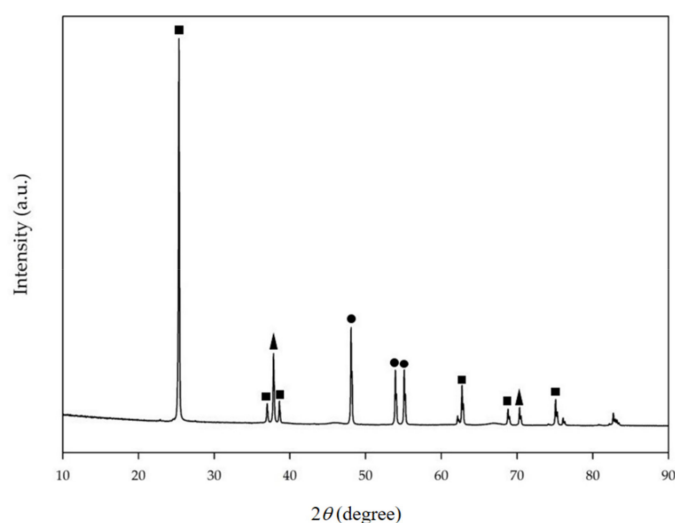


**Figure 5.** The diffraction peaks of the Pd/Al<sub>2</sub>O<sub>3</sub> catalyst analyzed by an X-ray diffractometer (● PdO, ▲ Al<sub>2</sub>O<sub>3</sub>, and ■ TiO<sub>2</sub>).

**Table 2.** Kerosene selectivity results for every run order designed by box-Behnken design (BBD).

Standard Order	Temperature (°C)	Pressure (MPa)	LHSV (h <sup>-1</sup> )	Kerosene Selectivity (%)
1	450	4	1.0	51.28
2	550	4	1.0	26.04
3	450	6	1.0	50.00
4	550	6	1.0	25.81
5	450	5	0.5	49.46
6	550	5	0.5	17.53
7	450	5	1.5	47.83
8	550	5	1.5	35.87
9	500	4	0.5	47.83
10	500	6	0.5	29.17
11	500	4	1.5	57.89
12	500	6	1.5	54.35
13	500	5	1.0	51.06
14	500	5	1.0	52.69
15	500	5	1.0	54.84

The ANOVA results of the significance of each variable with 95% confidence are presented in Table 3. We found that the linear, square, and interaction  $F_{\text{values}}$  were 23.20, 8.77, and 2.44, respectively. These indicate the significant effects of linear and square terms due to  $F_{\text{values}}$  being higher than  $F_{\text{critical}}$ , whereas  $F_{\text{critical}}$  at  $F_{(0.05, 3, 5)}$  was 5.41. These results were the same as those obtained for temperature and LHSV in the linear terms, including the square term of temperature. Conversely, the interaction term

and the linear term of pressure had insignificant effects ( $F_{\text{value}} < F_{\text{critical}}$ ). Even though researchers have studied the effects of parameters such as temperature, pressure, and reaction time on hydro-cracking by varying one factor at a time, they have reported that these might affect the product selectivity. Severe reaction conditions produce short hydrocarbon products due to the cracking phenomenon [24–26]. However, a key objective of this work was to confirm the experimental results using the DOE method, which could demonstrate both the significant effects of each parameter and those among interactions. The selection of a parameter's range should be specific for the response. In other words, the range of reaction conditions can impact the extent and selectivity of hydrocracking products, which can be optimised for BHK production. For instance, a higher pressure range might encourage the selectivity of gasoline or other light hydrocarbons instead of kerosene. Thus, the insignificant effects of pressure shown in the ANOVA (Table 3) could explain that the pressure range used in this work is suitable for kerosene production. We found that pressure has no impact on the BHK product. In addition, the interaction effects represent the combination effects of factors on the dependent variable, implying that if the impact of one factor depends on the other factors, a significant interaction effect would be found. Due to the insignificant effect of the interaction presented in Table 3, we concluded that the level of combined factors does not influence individual factors. This could be related to the square terms of each parameter, which showed that the square terms of pressure and LHSV had insignificant effects. Conversely, the reaction temperature has been confirmed to strongly impact hydro-cracking products in previous works [25–27]. All the mentioned results were confirmed by the  $P_{\text{value}}$ . The  $F_{\text{value}}$  of the lack-of-fit was 9.33 compared to the  $F_{\text{critical}}$  of the lack-of-fit ( $F_{(0.05, 3, 2)} = 19.16$ ). The  $F_{\text{value}}$  was less than the  $F_{\text{critical}}$  and the  $P_{\text{value}}$  was higher than 0.05 ( $P_{\text{value}} = 0.098$ ), confirming the insignificant effect of lack-of-fit. Thus, it can be concluded that the mathematical model can be used to explain experimental results because of the insignificant error of predicted results.

**Table 3.** Analysis of variance for kerosene selectivity.

Source	DF	$F_{\text{value}}$	$P_{\text{value}}$	Result
Regression	9	11.47	0.008	significant
Linear	3	23.20	0.002	significant
Temperature	1	50.64	0.001	significant
Pressure	1	3.27	0.130	insignificant
LHSV	1	15.70	0.011	significant
Square	3	8.77	0.020	significant
Temperature × Temperature	1	25.19	0.004	significant
Pressure × Pressure	1	1.05	0.353	insignificant
LHSV × LHSV	1	1.63	0.257	insignificant
Interaction	3	2.44	0.180	insignificant
Temperature × Pressure	1	0.01	0.915	insignificant
Temperature × LHSV	1	4.64	0.084	insignificant
Pressure × LHSV	1	2.66	0.164	insignificant
Residual Error	5			
Lack-of-Fit	3	9.33	0.098	insignificant
Pure error	2			
Total	14			
Source	DF1	DF2		$F_{\text{critical}}$
$F_{(0.05, DF1, DF2)}$	3	5		5.41
$F_{(0.05, DF1, DF2)}$	3	2		19.16

Legend: DF, degrees of freedom.

For the normality test, several points of the probability plot occurred along a straight line. The histogram shows the normal distribution of the standard residual. The standard error versus predicted results produced randomly scattered points around the zero line, and a similar trend was found in the standard residual versus observation (Figure S1). These results show that the standard residual calculated from difference between the predicted and experimental results supports a satisfactory

model and the experimental order had no significant error. In addition, we also confirmed the results as above by plotting the relationship between the estimated and actual experiments (Figure S2). The results showed that the correlative points lie along the regression line through the original. The coefficient of determination ( $R^2$ ) of kerosene selectivity was 87.07% due to the significant terms that were considered.

The interaction between all combined parameters are displayed as three-dimensional response surface plots (Figure 6). Figure 6a demonstrates the interaction between temperature and pressure. We found that kerosene selectivity increased as both parameters increased until it reached the highest value of nearly 60% at 480–500 °C and 5.0–5.5 MPa. Then, it decreased at temperatures over 500 °C and higher pressures, potentially because the substrate was converted to gasoline and others lighter gases instead of BHK. The results confirm the findings of previous studies in which it was reported that at high reaction temperature the initial alkanes underwent a cracking reaction to produce lighter hydrocarbons [25,28]. The same trend can be observed in Figure 6b: the kerosene selectivity increases as temperature and LHSV increase. The maximum kerosene selectivity was achieved, similar to Figure 6a, at the same temperature and 1.4 h<sup>-1</sup> LHSV. However, the temperature and LHSV were found to significantly affect the reaction; high temperature and low LHSV produce a high ratio of light hydrocarbons to gaseous products due to the harsh conditions and long reaction time [28,29]. Conversely, Figure 6c shows the fluctuating surface plot between pressure and LHSV. The tendency was, again, to be raised at the edge of the top range of pressure and LHSV. This likely occurred due to the selected range of both parameters, which may be inappropriate when combined during kerosene production. The interaction among parameters was also complex. In addition, it should be remarked that the ANOVA demonstrated the non-significant effect of the interaction of all parameters. However, the main essential parameters were temperature and LHSV, as indicated in the linear terms of individual parameters. This is in agreement with Bezergianni and Kalogianni, who studied the hydrocracking of used cooking oil for biofuel production. They reported that biofuel production is favored by increasing temperature and decreasing LHSV. However, moderate reaction temperatures and LHSVs were shown to be more attractive for diesel production (including kerosene production), whereas higher temperatures and lower LHSVs were more suitable for gasoline production [25]. This explains why Figure 6a,b show the same tendency due to both graphs being strongly affected by temperature in combination with other parameters, whereas Figure 6c is the opposite. However, the obtained model indicates that the suitable conditions for BHK production are about 483 °C, 5.0 MPa, and 1.4 h<sup>-1</sup>. These conditions could provide approximately 57.30% kerosene selectivity (Figure S3). For the kerosene yield, the result obtained under the optimal conditions was used to calculate the yield using Equation (3).

$$KY = (B/C) \times 100 \quad (3)$$

where  $KY$  is kerosene yield,  $B$  is the volume of the BHK fraction at the boiling point between 150 and 280 °C, and  $C$  is the RPO feed volume. The results show that under the optimal conditions, the kerosene yield was 47.76%. The yield and selectivity depend on the operating conditions. Due to the significant effects of the interaction between temperature and space velocity, high temperature and slow space velocity produced high amounts of light hydrocarbon and gaseous products. This finding agrees with that reported by Anand et al., who state that lower space velocities (1–3 h<sup>-1</sup>) and higher temperatures (>400 °C) are required to increase the yield of naphtha and kerosene-range hydrocarbons, whereas the partial pressure of hydrogen had a slight effect on the formation of the kerosene fraction at higher pressures [30].

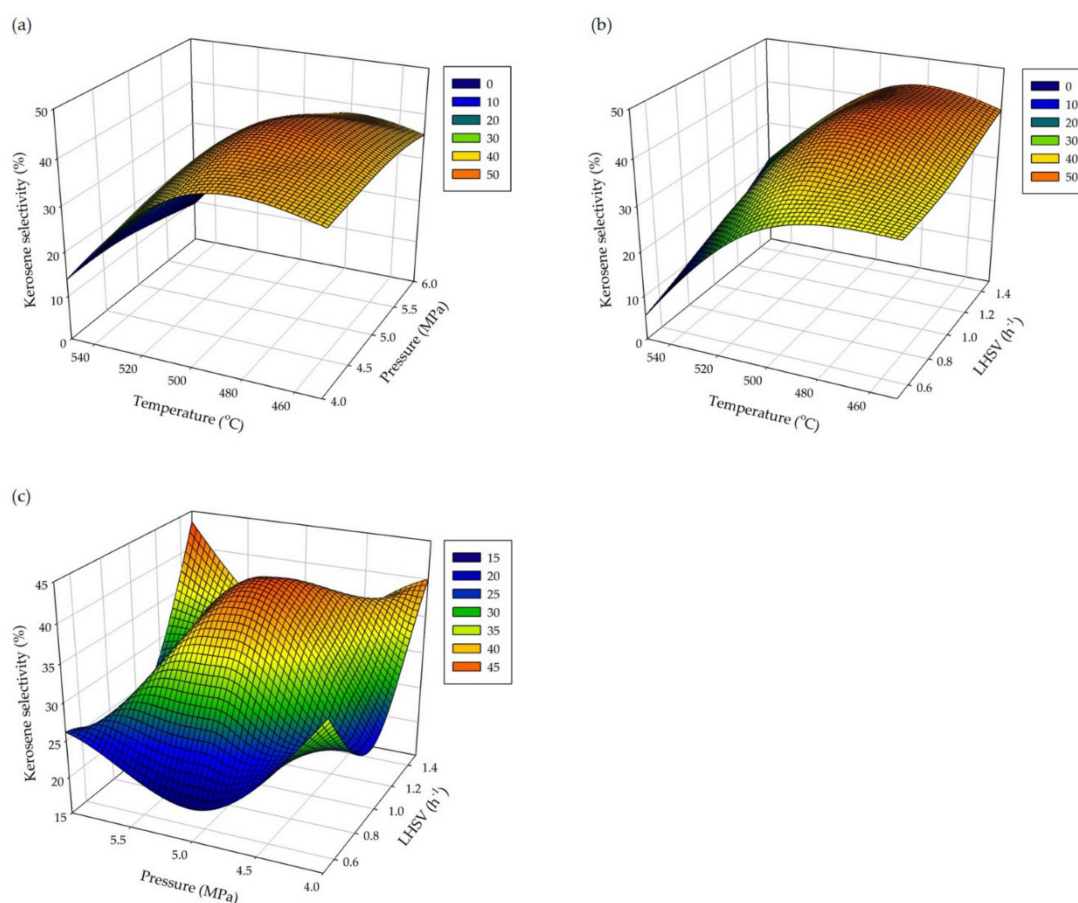


**Figure 6.** Response surface plots showing the effects of (a) temperature and pressure, (b) temperature and LHSV, and (c) pressure and LHSV on the production of kerosene selectivity via hydrocracking.

Table 4 compares the kerosene yield and selectivity values with those reported in the literature. Li et al. have investigated using palm oil as a feedstock for jet biofuel production via hydrocracking with different Ni-loaded zeolites. The highest kerosene yield was 42% when using Ni/SAPO-34 under the operating conditions of 390 °C, 3 MPa of H<sub>2</sub> pressure, and an eight-hour reaction time [31]. Other researchers have examined a variety of feed stocks. For example, hydrocracking of unrefined soybean oil under a zeolite ZSM-5 catalyst was examined and was found to yield 14.54% kerosene [32]. Verma et al. have studied the reaction of jatropha oil on sulfided NiW catalysts, and an 84% liquid hydrocarbon including that with a 37.5% kerosene range (C<sub>9</sub>–C<sub>14</sub>) were obtained under the operating conditions of 375–450 °C, 6–8 MPa, and 1 h<sup>-1</sup> in a fixed-bed reactor [9]. Wang et al. have reported the hydrotreatment of fatty acid methyl esters (FAME) to produce diesel-like hydrocarbons, and the lighter hydrocarbon in the kerosene range was derived from a cracking reaction. The highest light hydrocarbons (C<sub>9</sub>–C<sub>14</sub>) were produced at 33.2% under the catalytic conditions of Mo/Al<sub>2</sub>O<sub>3</sub> at 380 °C, 2 MPa of H<sub>2</sub> pressure, and a three-hour reaction time [33]. The use of FAME has also been studied by Chen et al. They investigated the conversion of FAME to alkane fuels by using a 10 wt.% Ni/HZSM-5 catalyst under the operating conditions of 280 °C, a H<sub>2</sub> pressure of 0.8 MPa, and an LHSV of 4 h<sup>-1</sup>. The maximum liquid alkane selectivity was found to be 88.2%, which included 32.5% kerosene [1]. Hengst et al. have investigated the deoxygenation of oleic acid over 1 wt.% palladium containing acidic catalysts. The product distribution of C<sub>10</sub>–C<sub>14</sub> was about 10% when the experiment was conducted at 380 °C, a weight hourly space velocity (WHSV) of 1.85 h<sup>-1</sup>, and ambient pressure [34]. Comparing these research works, we produced the highest kerosene yield and selectivity due to the high-temperature reaction that significantly affected BHK production in the optimization results. This optimal condition can be applied in future work.

**Table 4.** Comparative kerosene selectivity and yield from various feedstocks via catalytic cracking process with different catalysts and operating conditions.

Conditions	Feedstock	Catalysts	Kerosene		Ref.
			Yield (%)	Selectivity (%)	
483 °C, 5.0 MPa, and 1.4 h <sup>-1</sup> LHSV	RPO	Pd/Al <sub>2</sub> O <sub>3</sub>	47.46	57.30	This study
280 °C, 0.8 MPa, and LHSV 4 h <sup>-1</sup>	FAME	10 wt.% Ni/HZSM-5	NR	32.5	[1]
390 °C, 3 MPa, and 8-h RT	Palm oil	Ni/SAPO-34	42	69	[31]
450° C for 45 min with 0.07 g/min feed and gas flow rate 42 mL/min	Soybean oil	Zeolite ZSM-5	14.54	NR	[32]
450 °C, 6 MPa, and 1 h <sup>-1</sup> LHSV	Jatropha oil	NiW	37.5	NR	[9]
380 °C, 2 MPa, and 3 h RT	FAME	Mo/Al <sub>2</sub> O <sub>3</sub>	NR	33.2	[33]
		MoO/Al <sub>2</sub> O <sub>3</sub>	NR	25.79	
		Ni <sub>2</sub> P/Al <sub>2</sub> O <sub>3</sub>	NR	3.49	
		Mo <sub>2</sub> C/AC	NR	21.02	
		Mo/AC	NR	18.55	
MoS <sub>2</sub> /Al <sub>2</sub> O <sub>3</sub>	NR	11.89			
380 °C, WHSV 1.85 h <sup>-1</sup> , ambient pressure	Oleic acid	1 wt.% Pd/Siral70	NR	≈10 (C <sub>10</sub> –C <sub>14</sub> )	[34]

Legend: RT, reaction time; NR, not reported; FAME, fatty acid methyl esters; WHSV, weight hourly space velocity.

### 3.3. Bio-Hydrogenated Kerosene Properties

The crude biofuel collected directly from the HPPBR was continually refined and separated to purify BHK via a distillation process following the ASTM D86 method. The carbon atom composition of BHK was analyzed by gas chromatography, followed by the UOP915 method, with the result presented in Figure 7. We found that the carbon atom distribution was mainly in the range of C<sub>9</sub> to C<sub>16</sub>, which includes the range suitable for kerosene.

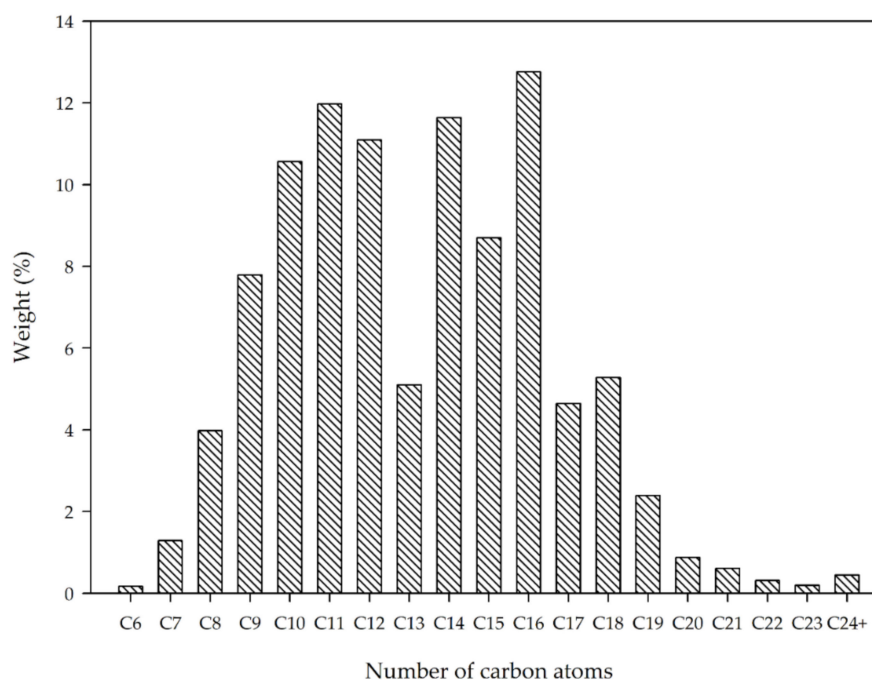
**Figure 7.** Number of carbon distribution as a function of percent by weight.

Table 5 characterizes BHK. Only the heating value and flash point met the standard requirements. The mass percentage of carbon and hydrogen was close to the requirement (99.1% versus 99.5%), whereas the oxygen and nitrogen were 0.8% and less than 0.1%, respectively. In addition, the reaction pathways can remove oxygen in the original feedstock and convert it to H<sub>2</sub>O, CO, and CO<sub>2</sub>. In brief, during the reaction mechanism for transforming TG into hydrocarbon, TG is broken down into various intermediates, which are presumed to be carboxylic acids. These intermediates are then converted into alkane hydrocarbons by three different pathways: decarboxylation, decarbonylation, and hydrodeoxygenation. These reactions can occur repeatedly as a loop during the reaction period. In the meantime, the fatty acids structure is broken down randomly and the carbon atom at the terminal of the hydrocarbon chain is removed first. This result is in agreement with Sankaranarayanan et al., who have reported that the double bonds present in the TG rapidly hydrogenated, saturating the TG structure, and then broke up into free fatty acids, which underwent either hydro-deoxygenation to produce *n*-paraffins and water with the same carbon number as the original fatty acid or decarboxylation/decarbonylation to produce *n*-paraffins with one carbon atom less and form CO and CO<sub>2</sub> as gaseous products. These reactions can occur directly through multiple cracking of TG molecules [35]. Huber et al. have reported that hydrogen is not required to convert a carboxylic acid group to an alkane by the decarboxylation pathway; hence, no water is produced from this pathway [36]. Therefore, we have concluded that some carbon could be lost in the formation of the gaseous products and is released from the reactor system along with vented gases.

**Table 5.** The physical and chemical properties of bio-hydrogenated kerosene (BHK) produced by hydrocracking compared to the specifications of kerosene-type aviation fuel MIL-DTL-83133H.

Property	Specification		BHK
	Min	Max	
Heat of combustion (MJ/kg)	42.8	-	45.8
Flash point (°C)	38	-	41
Freezing point (°C)	-	-47	-8
Carbon and hydrogen (mass percent)	99.5	-	99.1
Nitrogen (mass percent)	-	-	<0.10
Oxygen (mass percent)	-	-	0.8

In this work, the freezing value was higher than the requirement due to water formation. The distillation process could not completely eliminate water from the product. The high number of carbon atoms (C<sub>17</sub>–C<sub>24</sub>) in the carbon distribution profile affected the freezing point because they transform to the solid phase at low temperatures. Improving the freezing point will be investigated in future work. However, synthetic kerosene has been used to operate a commercial flight and a maximum 50/50 blend of synthetic kerosene and normal petroleum fuel was approved and granted certification to ensure supply security [37,38].

#### 4. Conclusions

In this work, RPO showed potential as feedstock for producing BHK via hydrocracking. Temperature and LHSV were found to be important reaction parameters because of their strongly significant effects, as indicated by the BBD results. The correlation between the estimated and actual values showed a good result; each correlative point lay along the regression line through the original and an  $R^2$  of 87.07% was obtained for the model. The optimal conditions of about 483 °C, 5.0 MPa, and 1.4 h<sup>-1</sup> were determined, which provided approximately 57.30% kerosene selectivity and 47.46% yield. The heating value and flash point met the standard specification. The mass percentages of carbon and hydrogen were 99.1% due to carbon loss in the reaction pathway forming CO and CO<sub>2</sub>. Water was also produced by the reaction, resulting in a high freezing point. Therefore, the properties of BHK should be improved in future work.

**Supplementary Materials:** The following are available online at <http://www.mdpi.com/1996-1073/12/16/3196/s1>, Figure S1: Residual plots of kerosene selectivity, Figure S2: Experimental and estimated results for kerosene selectivity, Figure S3: Optimal plot of kerosene selectivity.

**Author Contributions:** This research was conducted as a collaboration between all authors. P.D. proposed the methodology, conducted the experiment, and wrote the manuscript. A.N. proposed the methodology and numerical interpretation. P.K. was responsible for data analysis, discussion of results, and manuscript revision.

**Funding:** This research was funded by the Thailand Research Fund (TRF), Bangkok, Thailand, under the Royal Golden Jubilee Programme (RGJ; grant number PHD/0034/2556) and the Newton Fund, United Kingdom, for co-funding for a one-year PhD replacement in the UK.

**Acknowledgments:** This work was mainly supported by the Thailand Research Fund (TRF) Bangkok, Thailand under the Royal Golden Jubilee Programme (RGJ; grant number PHD/0034/2556) and the Newton Fund, United Kingdom, for co-funding under a travel bursary. In addition, Chumporn Palm Oil Industry, Chumporn, Thailand; The Royal Thai Air Force (RTAF), Bangkok, Thailand; and the Graduate School of Khon Kaen University, Khon Kaen, Thailand are also acknowledged for their materials and facilities support.

**Conflicts of Interest:** The authors declare no conflict of interest.

## References

1. Chen, L.; Li, H.; Fu, J.; Miao, C.; Lv, P.; Yuan, Z. Catalytic hydroprocessing of fatty acid methyl esters to renewable alkane fuels over Ni/HZSM-5 catalyst. *Catal. Today* **2016**, *259*, 266–276. [[CrossRef](#)]
2. Srifa, A.; Faungnawakij, K.; Itthibenchapong, V.; Viriya-empikul, N.; Charinpanitkul, T.; Assabumrungrat, S. Production of bio-hydrogenated diesel by catalytic hydrotreating of palm oil over NiMoS<sub>2</sub>/γ-Al<sub>2</sub>O<sub>3</sub> catalyst. *Bioresour. Technol.* **2014**, *158*, 81–90. [[CrossRef](#)]
3. Twaiq, F.A.; Mohamed, A.R.; Bhatia, S. Liquid hydrocarbon fuels from palm oil by catalytic cracking over aluminosilicate mesoporous catalysts with various Si/Al ratios. *Microporous Mesoporous Mater.* **2003**, *64*, 95–107. [[CrossRef](#)]
4. Vásquez, M.C.; Silva, E.E.; Castillo, E.F. Hydrotreatment of vegetable oils: A review of the technologies and its developments for jet biofuel production. *Biomass Bioenergy* **2017**, *105*, 197–206. [[CrossRef](#)]
5. Gutiérrez-Antonio, C.; Gómez-Castro, F.I.; De Lira-Flores, J.A.; Hernández, S. A review on the production processes of renewable jet fuel. *Renew. Sustain. Energy Rev.* **2017**, *79*, 709–729. [[CrossRef](#)]
6. Ancheyta, J.; Sánchez, S.; Rodríguez, M.A. Kinetic modeling of hydrocracking of heavy oil fractions: A review. *Catal. Today* **2005**, *109*, 76–92. [[CrossRef](#)]
7. Looi, P.Y.; Mohamed, A.R.; Tye, C.T. Hydrocracking of residual oil using molybdenum supported over mesoporous alumina as a catalyst. *Chem. Eng. J.* **2012**, *181–182*, 717–724. [[CrossRef](#)]
8. Serrano, D.P.; Escola, J.M.; Briones, L.; Arroyo, M. Hydroprocessing of the LDPE thermal cracking oil into transportation fuels over Pd supported on hierarchical ZSM-5 catalyst. *Fuel* **2017**, *206*, 190–198. [[CrossRef](#)]
9. Verma, D.; Rana, B.S.; Kumar, R.; Sibi, M.G.; Sinha, A.K. Diesel and aviation kerosene with desired aromatics from hydroprocessing of jatropha oil over hydrogenation catalysts supported on hierarchical mesoporous SAPO-11. *Appl. Catal. A Gen.* **2015**, *490*, 108–116. [[CrossRef](#)]
10. Mat Yasin, M.H.; Mamat, R.; Najafi, G.; Ali, O.M.; Yusop, A.F.; Ali, M.H. Potentials of palm oil as new feedstock oil for a global alternative fuel: A review. *Renew. Sustain. Energy Rev.* **2017**, *79*, 1034–1049. [[CrossRef](#)]
11. Chowdhury, K.; Banu, L.; Khan, S.; Latif, A. Studies on the Fatty Acid Composition of Edible Oil. *Bangladesh J. Sci. Ind. Res.* **1970**, *42*, 311–316. [[CrossRef](#)]
12. Aslan, N.; Cebeci, Y. Application of Box-Behnken design and response surface methodology for modeling of some Turkish coals. *Fuel* **2007**, *86*, 90–97. [[CrossRef](#)]
13. Dujjanutat, P.; Neramittagapong, A.; Kaewkannetra, P. H<sub>2</sub>-assisted chemical reaction for green-kerosene production. *Defect Diffus. Forum* **2015**, *364*, 104–111. [[CrossRef](#)]
14. Ferris, A.M.; Rothamer, D.A. Methodology for the experimental measurement of vapor-liquid equilibrium distillation curves using a modified ASTM D86 setup. *Fuel* **2016**, *182*, 467–479. [[CrossRef](#)]
15. Groen, J.C.; Peffer, L.A.A.; Pérez-Ramírez, J. Pore size determination in modified micro- and mesoporous materials. Pitfalls and limitations in gas adsorption data analysis. *Microporous Mesoporous Mater.* **2003**, *60*, 1–17. [[CrossRef](#)]

16. Tiwari, R.; Rana, B.S.; Kumar, R.; Verma, D.; Kumar, R.; Joshi, R.K.; Garg, M.O.; Sinha, A.K. Hydrotreating and hydrocracking catalysts for processing of waste soya-oil and refinery-oil mixtures. *Catal. Commun.* **2011**, *12*, 559–562. [[CrossRef](#)]
17. Callejas, M.A.; Martínez, M.T.; Blasco, T.; Sastre, E. Coke characterisation in aged residue hydrotreating catalysts by solid-state <sup>13</sup>C-NMR spectroscopy and temperature-programmed oxidation. *Appl. Catal. A Gen.* **2001**, *218*, 181–188. [[CrossRef](#)]
18. Vozka, P.; Orazgaliyeva, D.; Šimáček, P.; Blažek, J.; Kilaz, G. Activity comparison of Ni-Mo/Al<sub>2</sub>O<sub>3</sub> and Ni-Mo/TiO<sub>2</sub> catalysts in hydroprocessing of middle petroleum distillates and their blend with rapeseed oil. *Fuel Process. Technol.* **2017**, *167*, 684–694. [[CrossRef](#)]
19. Breyse, M.; Portefaix, J.L.; Vrinat, M. Support effects on hydrotreating catalysts. *Catal. Today* **1991**, *10*, 489–505. [[CrossRef](#)]
20. Morales-Ortuño, J.C.; Klimova, T.E. Development of new hydrodesulfurization NiMo catalysts supported on Al<sub>2</sub>O<sub>3</sub>-TiSBA-15 hybrid materials. *Fuel* **2017**, *198*, 99–109. [[CrossRef](#)]
21. Morales-Ortuño, J.C.; Ortega-Domínguez, R.A.; Hernández-Hipólito, P.; Bokhimi, X.; Klimova, T.E. HDS performance of NiMo catalysts supported on nanostructured materials containing titania. *Catal. Today* **2016**, *271*, 127–139. [[CrossRef](#)]
22. Castillo-Villalón, P.; Ramírez, J.; Cuevas, R.; Vázquez, P.; Castañeda, R. Influence of the support on the catalytic performance of Mo, CoMo, and NiMo catalysts supported on Al<sub>2</sub>O<sub>3</sub> and TiO<sub>2</sub> during the HDS of thiophene, dibenzothiophene, or 4,6-dimethylbenzothiophene. *Catal. Today* **2016**, *259*, 140–149. [[CrossRef](#)]
23. Liu, C.; Zhou, Z.; Huang, Y.; Cheng, Z.; Yuan, W. Support effects on thiophene hydrodesulfurization over Co-Mo-Ni/Al<sub>2</sub>O<sub>3</sub> and Co-Mo-Ni/TiO<sub>2</sub>-Al<sub>2</sub>O<sub>3</sub> catalysts. *Chin. J. Chem. Eng.* **2014**, *22*, 383–391. [[CrossRef](#)]
24. Chu, P.L.; Vanderghem, C.; MacLean, H.L.; Saville, B.A. Process modeling of hydrodeoxygenation to produce renewable jet fuel and other hydrocarbon fuels. *Fuel* **2017**, *196*, 298–305. [[CrossRef](#)]
25. Bezergianni, S.; Kalogianni, A. Hydrocracking of used cooking oil for biofuels production. *Bioresour. Technol.* **2009**, *100*, 3927–3932. [[CrossRef](#)] [[PubMed](#)]
26. Kiatkittipong, W.; Phimsen, S.; Kiatkittipong, K.; Wongsakulphasatch, S.; Laosiripojana, N.; Assabumrungrat, S. Diesel-like hydrocarbon production from hydroprocessing of relevant refining palm oil. *Fuel Process. Technol.* **2013**, *116*, 16–26. [[CrossRef](#)]
27. Xu, J.; Jiang, J.; Zhao, J. Thermochemical conversion of triglycerides for production of drop-in liquid fuels. *Renew. Sustain. Energy Rev.* **2016**, *58*, 331–340. [[CrossRef](#)]
28. Galadima, A.; Muraza, O. Catalytic upgrading of vegetable oils into jet fuels range hydrocarbons using heterogeneous catalysts: A review. *J. Ind. Eng. Chem.* **2015**, *29*, 12–23. [[CrossRef](#)]
29. Bezergianni, S.; Kalogianni, A.; Vasalos, I.A. Hydrocracking of vacuum gas oil-vegetable oil mixtures for biofuels production. *Bioresour. Technol.* **2009**, *100*, 3036–3042. [[CrossRef](#)] [[PubMed](#)]
30. Anand, M.; Farooqui, S.A.; Kumar, R.; Joshi, R.; Kumar, R.; Sibi, M.G.; Singh, H.; Sinha, A.K. Optimizing renewable oil hydrocracking conditions for aviation bio-kerosene production. *Fuel Process. Technol.* **2016**, *151*, 50–58. [[CrossRef](#)]
31. Li, T.; Cheng, J.; Huang, R.; Yang, W.; Zhou, J.; Cen, K. Hydrocracking of palm oil to jet biofuel over different zeolites. *Int. J. Hydrog. Energy* **2016**, *41*, 21883–21887. [[CrossRef](#)]
32. Emori, E.Y.; Hirashima, F.H.; Zandonai, C.H.; Ortiz-Bravo, C.A.; Fernandes-Machado, N.R.C.; Olsen-Scaliente, M.H.N. Catalytic cracking of soybean oil using ZSM5 zeolite. *Catal. Today* **2017**, *279*, 168–176. [[CrossRef](#)]
33. Wang, F.; Xu, J.; Jiang, J.; Liu, P.; Li, F.; Ye, J.; Zhou, M. Hydrotreatment of vegetable oil for green diesel over activated carbon supported molybdenum carbide catalyst. *Fuel* **2018**, *216*, 738–746. [[CrossRef](#)]
34. Hengst, K.; Arend, M.; Pfützenreuter, R.; Hoelderich, W.F. Deoxygenation and cracking of free fatty acids over acidic catalysts by single step conversion for the production of diesel fuel and fuel blends. *Appl. Catal. B Environ.* **2015**, *174–175*, 383–394. [[CrossRef](#)]
35. Sankaranarayanan, T.M.; Banu, M.; Pandurangan, A.; Sivasanker, S. Hydroprocessing of sunflower oil-gas oil blends over sulfided Ni-Mo-Al-zeolite beta composites. *Bioresour. Technol.* **2011**, *102*, 10717–10723. [[CrossRef](#)]
36. Huber, G.W.; O'Connor, P.; Corma, A. Processing biomass in conventional oil refineries: Production of high quality diesel by hydrotreating vegetable oils in heavy vacuum oil mixtures. *Appl. Catal. A Gen.* **2007**, *329*, 120–129. [[CrossRef](#)]

37. Chuck, C.J.; Donnelly, J. The compatibility of potential bioderived fuels with Jet A-1 aviation kerosene. *Appl. Energy* **2014**, *118*, 83–91. [[CrossRef](#)]
38. Rye, L.; Blakey, S.; Wilson, C.W. Sustainability of supply or the planet: A review of potential drop-in alternative aviation fuels. *Energy Environ. Sci.* **2010**, *3*, 17–27. [[CrossRef](#)]



© 2019 by the authors. Licensee MDPI, Basel, Switzerland. This article is an open access article distributed under the terms and conditions of the Creative Commons Attribution (CC BY) license (<http://creativecommons.org/licenses/by/4.0/>).